Preparation of Fully Bio-based Sound Absorbers from Waste Wood and Pulp Fibers by Foam Forming

Mikko J. Valkonen,[a] Jose Cucharero,[b,c] Tapio Lokki,[c] Lauri Rautkari,[a] and Tuomas Hänninen [b,*]

Building materials that are bio-based and produced from waste streams have a substantial effect on the carbon footprint of buildings. In this study, the authors prepared fully bio-based sound absorbers from waste wood and other cellulosic materials. Cutter shavings (CSs), softwood pulp, and cellulose powder (CP) were used as raw materials to prepare sound absorber samples using the foam-forming technique. The fully bio-based sound absorbers prepared were mechanically stable. However, an increase in CSs content decreased their mechanical properties, and samples with high CSs content became difficult to handle. The CP increased the mechanical properties, but it did not affect the sound absorption of the samples. The sound absorption properties of these fully bio-based materials could be tuned by carefully selecting CSs and fiber contents and adjusting the thickness of the material. Greater CSs content decreased the sound absorption properties of the materials. This decrease was mainly due to an increase in the average pore size, leading to poorer sound energy dissipation by visco-thermal effects.

*Contact information: a: Department of Bioproducts and Biosystems, School of Chemical Engineering, Aalto University, P.O. Box 16300, 00076 Aalto, Finland; b: Lumir Oy, Linjatie 2, 01260 Vantaa, Finland; c: Department of Signal Processing and Acoustics, School of Electrical Engineering, Aalto University, P.O. Box 13100, 00076 Aalto, Finland; *Corresponding author: tuomas.hanninen@lumir.fi*

INTRODUCTION

Excessive amounts of waste wood are generated by lumber, packaging, and construction industries. Much of this is presently used for energy production by incineration. Utilization of such waste in long-life products, such as construction materials, could be used to sequester the CO_2 and decrease CO_2 emissions. The primary constraint for recycling wood by-products is the possible contamination of the material, which reduces the probability of utilizing it without additional processing. Nevertheless, waste wood recycling has been prioritized over incineration to produce energy and landfilling strategies (Garcia and Hora 2017; Hassan *et al.* 2019).

In this study, the authors demonstrated the possibility to utilize waste wood in the preparation of fully bio-based sound absorbers. Traditionally porous sound absorbers are produced from glass or rock wool, which currently can be made from recycled raw material. Manufacturing traditional sound absorbers, however, requires much energy. Therefore, they have a remarkably higher environmental impact than bio-based raw materials, which do not require much energy in the manufacturing process and sequester the carbon into buildings, which in the best cases last for decades.

Focus on reducing the environmental impacts of the construction industry has primarily been in the operational energy efficiency of the buildings and the use of renewable energy. However, as buildings' energy use becomes more sustainable, the proportional impact of building materials is increasing.

Low-embodied energy building materials produced from recycled wood are an environmentally friendly alternative, saving virgin raw materials and minimizing emissions while acting as carbon sinks during their operating life. Such materials are needed to reduce the role of buildings in global warming and attain more remarkable CO_2 sequestration than emissions (Ibn-Mohammed *et al.* 2013; Hill 2019).

To function effectively as a sound absorber, the material must have the capability to absorb most of the sound energy that hits its surface (Jahangiri *et al.* 2016). Porous sound absorbers consist of open-cell foams and fibrous or granular materials. The main mechanisms of sound energy dissipation in porous materials are viscous effects associated with the relative motion between air molecules and the solid walls, thermal effects related to heat exchange between air molecules and the solid walls, and inertial effects associated with changes in the motion of air particles, thus causing a loss of momentum in the direction of wave propagation (Attenborough 1971; Fahy 2000). Typically, granular porous materials with larger pores present an additional sound absorption mechanism. Such a mechanism is related to a destructive interference occurring at the surface of the material between the direct and the reflected sound waves from the rigid backing behind the samples. This resonance plays a relevant role when the visco-thermal losses inside the material are insufficient to attenuate the sound wave reflected from the rigid backing completely (Swift *et al.* 1999).

The authors produced fully bio-based sound absorbers consisting of granular and fibrous particles from a mixture of waste cutter shavings (CSs), softwood (SW) pulp, and cellulose powder (CP). Bio-based sound absorbing samples were produced using the foam-forming technique. Foam forming technology involves the mixing of fibres, water and a foaming agent to create a wet foam. Bubbles prevent flocculation of fibres, which form an open cell fibrous foam upon drying (Hjelt *et al.* 2022). Cellulosic particles are bound together mainly by hydrogen bonds in the dry 3D structure. Earlier studies have shown that foams produced from pulp perform well as sound absorbers (Jahangiri *et al.* 2016; Pöhler *et al.* 2016; Cucharero *et al.* 2020, 2021; Dong *et al.* 2021). Sound absorption and mechanical properties were studied to evaluate different material combinations.

EXPERIMENTAL

Materials

Cutter shavings (South-Eastern Finland University of Applied Sciences Ltd. Wood Technology Laboratory, Mikkeli, Finland), bleached SW kraft pulp (pulp mill in southern Finland), and CP (Arbocel®, JRS - J. Rettenmaier & Söhne GmbH + Co KG, Rosenberg, Germany) were used as raw materials for foams (Table 1). The CSs were a mixture of different wood species. Sodium dodecyl sulfate (SDS) (dry fatty alcohol sulphate 80 to 100%, Unger Fabrikker AS, Gamle Fredrikstad, Norway) was used as a foaming agent.

Methods

Foam forming

The CSs, SW pulp, and CP were weighed first (Table 1), and the CSs and SW pulp were soaked overnight in 10 L of water. The suspension was mixed for 5 min to thoroughly disperse the components. 2.3 g of SDS was added, and the suspension was foamed with a mixer until the volume of the mixture was doubled. The mixer was built following (Lappalainen and Lehmonen 2012). After foam forming, the foam was poured in a square mold of dimensions 40 cm x 40 cm x 50 cm with two stainless still nets located at the bottom. The top net had an opening mesh of 0.16 mm, while the net below had an opening mesh of 5 mm. The latter served as support for the top net to avoid curvature of materials. The mold was gently shaken to distribute the foam more evenly in the mold, and then the foam was left to gravity drain for 15 min. The wet foams were solidified by drying them with airflow at 40 to 50 °C in ambient conditions for 3 to 5 days. The dry foams were rewetted by spraying a small amount of water on the samples and compressed for 1 to 2 days evenly to 50 mm thickness. A photograph of the samples is shown in Fig. 1. The samples had been cut to size for impedance tube measurements.

Fig. 1. Samples with increasing CSs content from left to right (S1 to S5). The samples with a lower CP content (sample A) are in the front row. A loose sample of CSs was placed in front of the samples. The samples were cut to size for impedance tube measurements

The particle size distribution of the cutter shavings

The particle size distribution of the CSs was analyzed using a Retsch AS 300 Control Vibratory Sieve Shaker (Retsch GmbH, Haan, Germany) from 25 g of CSs with 180, 250, 355, 500, and 710 μm, and 1.0, 1.4, 2.0, 2.8, 4.0, 5.6, 8.0, and 11.2 mm sieves. The separated CSs were then weighed after sieving. The mass fraction of retained CSs ($m_{R,i}$, %) was calculated following Eq. 1,

$$m_{R,i} (\%) = 100 m_{R,i} / \Sigma m_R \tag{1}$$

where $m_{R,i}$ is the retained mass per a given sieve size as dry matter content (g) and Σm_R is the total retained mass (g).

Compression testing and related physical properties determination

Compression testing was performed according to SFS-EN 826 (2013) using a Zwick MTS 1475 universal material testing machine (Zwick Roell Group, Ulm, Germany) with TestWorks® 4 software (MTS Systems Corporation, Eden Prairie, MN, USA). Three 100×100 mm^2 samples were prepared with a band saw from the foams. The samples were conditioned in *ca.* 65% relative humidity (RH) at 20 °C overnight in a conditioning room. The initial load was *ca.* 2.5 N, and the rate of compression used was 5 mm/min. The samples were initially compressed to 10% strain following a 1.0 min relaxation time and compression to 50% strain. The compression modulus of elasticity (E, kPa) was calculated following Eq. 2 (Celzard *et al.* 2010),

$$E = (\sigma_{10} - \sigma_4) / (\varepsilon_{10(\%)} - \varepsilon_{4(\%)}) \tag{2}$$

where σ_{10} and σ_4 are stresses at 4% and 10% strain (kPa), respectively, and ε_4 and ε_{10} are 4% and 10% strain (%), respectively. The compression modulus of elasticity is the slope of the formed line. The maximum stress was used to calculate the compressive strength at 50% strain and specific compressive strength at 50% strain. The specific compressive strength (σ_s, Nm/g) was determined following Eq. 3,

$$\sigma_s = \sigma_{50} / \rho \tag{3}$$

where σ_{50} is stress at 50% strain (Pa) and ρ is the bulk density of a dry sample (g/m^3). Recovery of the samples was measured after one week from the thickness of the samples.

Sound absorption coefficient determination

Samples were prepared for sound absorption measurement by cutting them to size and adjusting the thickness to 45 mm by removing 5 mm in total from both sides of the sample to remove the effects of a density gradient caused by the compression. The sound absorption coefficient was determined according to SFS-EN ISO 10534-2 (2001). The impedance tube used was a Brüel & Kjær Type 4206 (Brüel & Kjær Sound & Vibration Measurement, Nærum, Denmark). Two measurements were taken for each sample with the large impedance tube (100-mm tube diameter) and two to four measurements with the small impedance tube (29-mm tube diameter), providing results in the frequency range 100 to 1600 Hz and 500 to 6000 Hz, respectively. Samples consisting of 100% CSs were measured as loose particles with the impedance tube vertically mounted.

RESULTS AND DISCUSSION

Particle Size Distribution Results of the Cutter Shavings

The particle size distribution results are shown in Fig. 2. Approximately 70% of the retained mass was in the 1.4 mm to 5.6 mm particle size range. The particle sizes of the CSs were remarkably larger than those of the other components of the foams. The size less than 1.4 mm fraction consisted of fine particles characterized by their high surface area. Such fine particles might have some relevance to the formation of the foam despite their small share (*ca.* 17%), as they may interact with the surfactant.
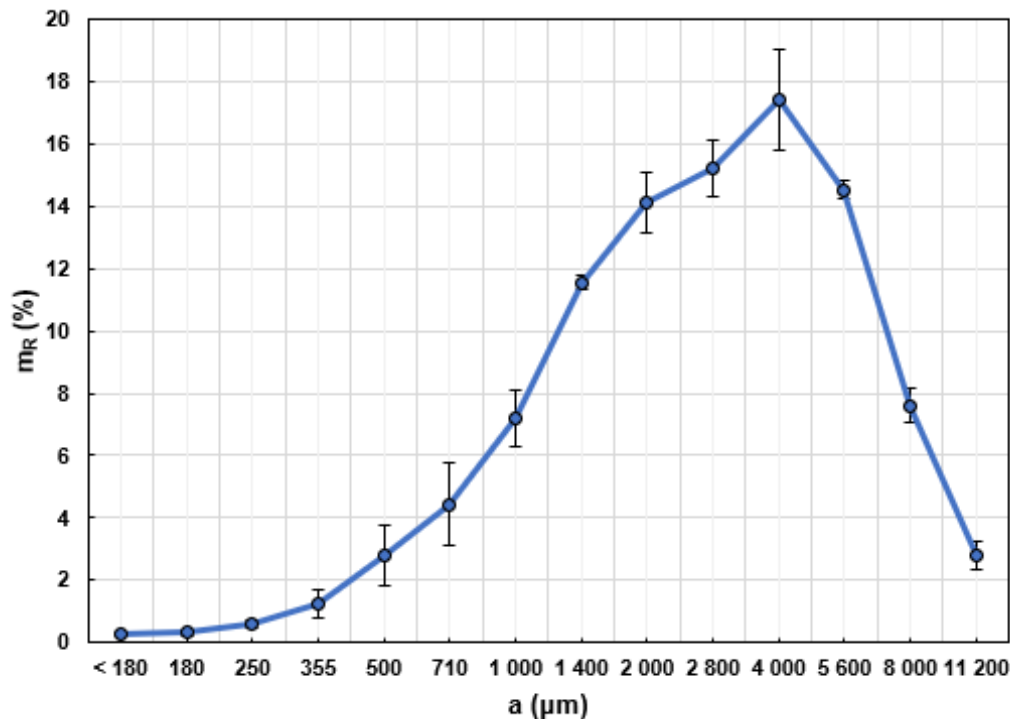
Fig. 2. The mass fraction of retained CSs (m_R) with residuals, *i.e.*, mass losses considered per sieve size (a); error bars depict the sample standard deviations of the retained mass fractions

Compression Testing and Related Physical Properties Results

Sufficient mechanical properties are a prerequisite for handling and installing building materials. The bulk densities, compressive strengths, specific compressive strengths, compression moduli of elasticity, and recovery of the samples are presented in Table 1. The densities of the samples were often higher compared to values of the foam-formed structures in the literature (Ketoja *et al.* 2019; Pöhler *et al.* 2020; Cucharero *et al.* 2021). The samples with high CSs content (the S5 samples) crumbled when handled. The CP did not affect the handling of the samples. Requirements for mechanical properties of building materials depends on how product is used. For acoustic materials to be used as building material in larger scale, they will need to remain stable in various kinds of installation systems (glued, mechanically attached, suspended ceiling systems, *etc.*). Testing these kinds of systems was not included in this paper.

The compressive strength, specific compressive strength, and compression modulus of elasticity seemed to decrease with an increasing ratio of CSs. These decreases are attributed to the decrease in the bonding contact area between the particles. The poor adhesion between the SW pulp and the CSs also plays a role. The surface of the CS particles consists of cellulose, lignin, and possibly small quantities of extractives. Cellulosic fibers form hydrogen bonds and adhere to each other upon drying, while the adhesion between cellulose and lignin or extractives is remarkably poorer (Notley and Norgren 2006). The results indicate that the fiber network is the structure that contributes most to the mechanical properties of the SW pulp – CSs foams. The CSs can be considered weak points or defects in the fiber network (Alava and Niskanen 2006).

In all the cases, a higher CP content increased the compressive and specific compressive strength properties (Table 1). A similar improvement of mechanical properties by micro- and nano-fibrillated cellulosic particles was reported by Pöhler *et al.*

(2020). The CP increased the strength properties by acting as a binder agent between the SW pulp fibers as it is transported to the interfiber joints, increasing the bonded area between the fibers (Paunonen *et al.* 2018). A stronger interfiber bonding enables the fibers to bear higher loads in compression. The effect can also be seen in the compression modulus of elasticity results (Table 1). However, the effect became less prominent as the CSs content of the samples increased. These observations indicate that the CP improved the bonding between the fibers but not between the fibers and CS particles.

Table 1. The CSs (m_{CSs}), SW pulp ($m_{SW\ pulp}$), and CP (m_{CP}) Contents (g of oven-dry) of the Samples, Bulk Densities (ρ), Compressive Strengths Until 50% Strain (σ_{50}), Specific Compressive Strengths Until 50% Strain ($\sigma_{s,50}$), Compression Moduli of Elasticity (E), and Recovery After One Week (R) of the Samples

Sample	m_{CSs} (g)	$m_{SW\ pulp}$ (g)	m_{CP} (g)	ρ (kg/m^3)	σ_{50} (kPa)	$\sigma_{s,50}$ (Nm/g)	E (kPa)	R (%)
S1A	0.0	534.6	112.6	87.9 (12.3)	227.3 (55.6)	2.6 (0.6)	481.9 (45.5)	73.7 (3.0)
S1B	0.0	534.6	168.9	91.8 (4.9)	228.3 (21.7)	2.5 (0.2)	496.7 (61.3)	70.3 (3.6)
S2A	108.4	427.6	112.9	89.9 (1.9)	152.7 (11.0)	1.7 (0.1)	283.0 (20.4)	74.4 (1.0)
S2B	108.4	427.6	169.6	94.2 (0.9)	209.3 (6.1)	2.2 (0.1)	359.3 (5.6)	73.9 (0.7)
S3A	216.7	320.7	113.3	82.5 (1.8)	164.7 (5.5)	2.1 (0.1)	270.2 (18.5)	70.6 (1.0)
S3B	216.7	320.7	169.7	89.5 (4.4)	179.3 (19.1)	2.0 (0.2)	267.6 (17.2)	69.9 (6.2)
S4A	298.0	240.6	113.4	82.6 (2.7)	130.0 (13.1)	1.6 (0.2)	200.9 (8.6)	63.3 (0.4)
S4B	298.0	240.6	170.1	87.8 (4.4)	159.7 (8.1)	1.8 (0.1)	224.0 (22.8)	65.6 (4.6)
S5A	379.2	160.4	113.9	82.4 (1.4)	114.0 (7.0)	1.4 (0.1)	173.5 (6.9)	63.7 (4.4)
S5B	379.2	160.4	170.5	91.9 (1.3)	155.0 (13.2)	1.7 (0.1)	190.2 (15.6)	68.8 (0.9)

Notes: Sample standard deviations are presented in parentheses.

The CSs seemed to slightly decrease the recovery of the samples (Table 1), which could be explained by the weaker fiber network for the high CSs samples. The buckling deformation of the fibers likely caused the inelastic deformation of the samples. The CP content did not remarkably affect the recovery, which would indicate that inelastic deformation is attributed to fiber bending rather than interfiber bond breakage or bond opening (Paunonen *et al.* 2018; Pöhler *et al.* 2020).

The stress-strain curves up to 50% strain of the samples with two CP contents is shown in Fig. 3. The shape of the curves agrees well with the literature (Ferreira and Rezende 2018; Pöhler *et al.* 2020). The elastic region is identified at low compressions with strain less than 10%. The compression modulus was defined as the steepest slope found in the elastic region, 4 to 10% strain (Celzard *et al.* 2010). The beginning of the elastic region, 0 to 4% strain, is attributed to the parallelization of the opposite surfaces subjected to compressive stress (Celzard *et al.* 2010). After the elastic region, the material starts to absorb the energy by plastic deformation caused by the fiber deformation and failure of interfiber bonds (Ashby 1983). The reinforcing effect of CP in sample S2B can

be seen clearly in Fig. 3 as higher stress values after the elastic region. The samples with a higher CSs content (S4A and S4B) follow the same trend as other samples. The CP reinforces the samples; however, the effect is more negligible. Figure S1 in the supplementary material presents the averaged stress-strain curves for all the samples.
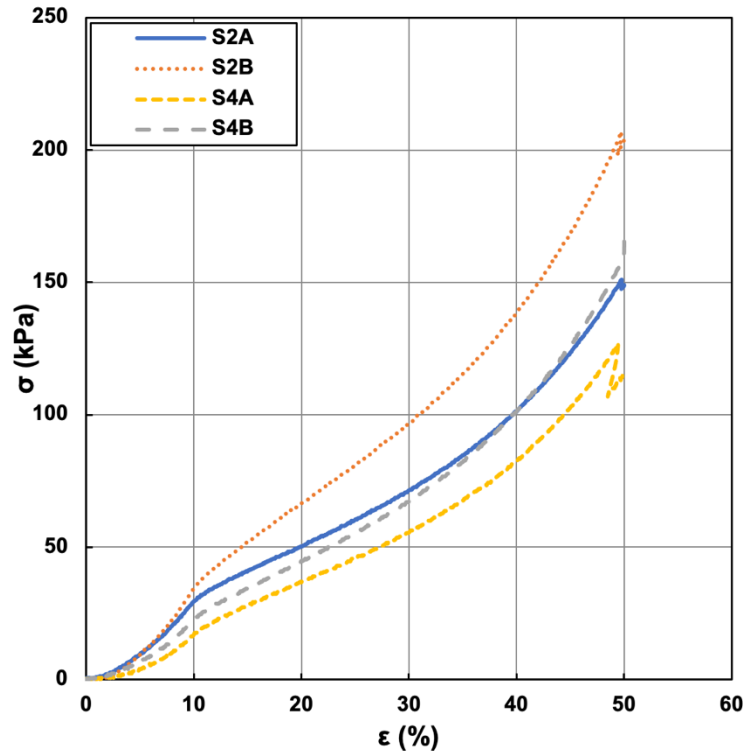

Fig. 3. Stress (σ) – strain (ε) curve until 50% strain for samples S2A, S2B, S4A, and S4B

Sound Absorption Coefficient Results

The sound absorption coefficients of the samples are illustrated in Figs. 4 and 5 for the frequency ranges of 100 to 1600 Hz and 500 to 6000 Hz, respectively. The first absorption peak detected in the absorption spectra is mainly related to the thickness of the material for the above frequency ranges. Both figures show that there was a trend in the results suggesting that increasing the CSs content in the materials shifts the first absorption peak to higher frequencies and thus results in poorer absorption at lower frequencies.

The absorption spectra curves of the samples containing only CSs present strong resonances/peaks at specific frequencies. These resonances indicate that losses of sound energy in the material due to visco-thermal effects were poor and that the primary mechanism for sound absorption is caused by the interference between the direct and reflected sound from the rigid backing of the material (Swift *et al.* 1999; Yamaguchi *et al.* 1999). For the samples with a lower CSs content, the absorption spectra curves flattened once the first peak was passed. This flattening indicates that for materials with a greater pulp fiber ratio, the contribution of visco-thermal effects to sound absorption became more relevant.
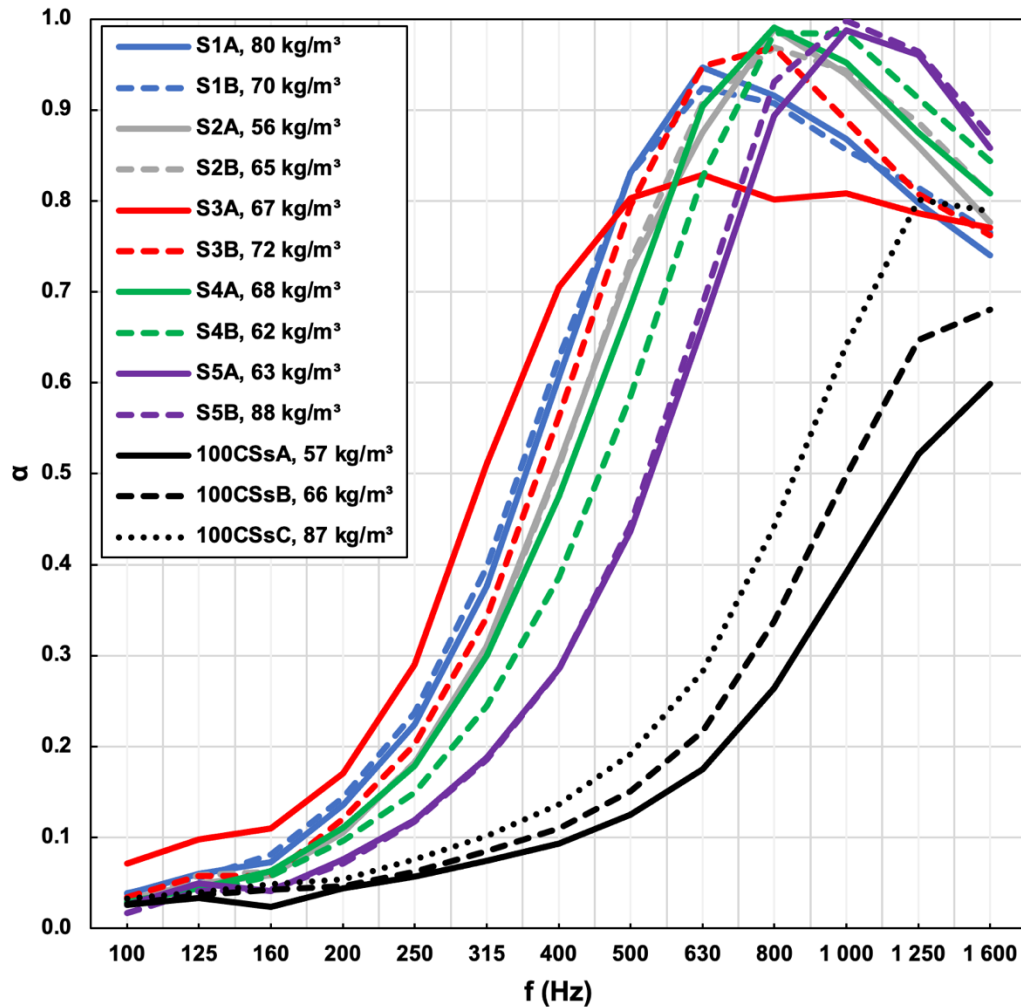
Fig. 4. Sound absorption coefficient (α) as a function of frequency (*f*) measured with large impedance tube; the sample bulk density is provided in the legend per case

The poorer sound absorption given by the samples containing only CSs is mainly explained by the large pores formed in the structure, leading to low flow resistivity, *i.e.*, low resistance of the material to a constant airflow. An increase in the density of the CSs samples results in increased absorption and shifting of the first absorption peak towards lower frequencies. The increase in absorption can be attributed to more remarkable visco-thermal effects in the porous structure due to smaller pore size and higher internal surface area. The increase in tortuosity can explain the shifting of the first absorption peak toward lower frequencies (Botterman *et al.* 2018). Tortuosity corresponds to the length of the sound path through the porous structure compared to the thickness of the material. Thus, the longer the sound passages compared to the thickness of the materials are, the greater the tortuosity, which results in the first absorption peaks located at lower frequencies. As the visco-thermal effects inside the porous structure increase, the relevance of the sound absorption mechanism related to the interference between the direct and reflected sound from the rigid backing lessens (Swift *et al.* 1999).
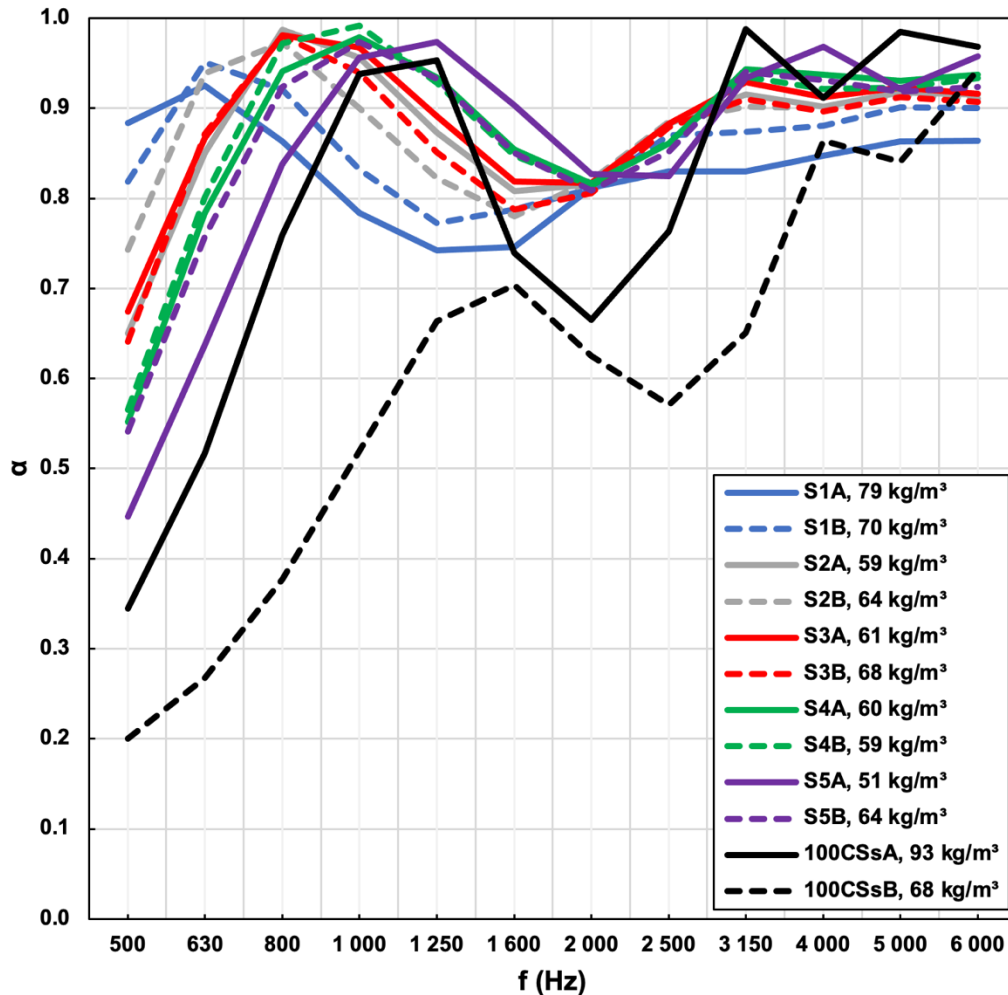
Fig. 5. Sound absorption coefficient (α) as a function of frequency (*f*) measured with small impedance tube; the sample bulk density is provided in the legend per case

The sound absorption properties of the samples prepared from a mixture of SW pulp fibers and CSs are governed by the fiber network rather than the granular structure. For these samples, the sound absorption was greater, and the first absorption peak was found at lower frequencies. The absorption curves of these samples flattened after the first absorption peak, which indicates that the visco-thermal effects were the dominating sound absorption mechanisms. Similar results were found in Cucharero *et al.* (2021). The first absorption peak moved towards lower frequencies as the content of the SW pulp fibers increased. This phenomenon can be associated with an increase in tortuosity as the decrease in the CSs content leads to structures with a smaller number of larger pores. Sample S3A in Fig. 4 presents a much reduced first absorption peak, which does not correlate with the general trend detected for all other samples. This anomaly could be because of the presence of inhomogeneity in the sample. Variations in the CP content did not remarkably influence the sound absorption properties of the materials.

Impedance tube measurements of absorption coefficients for frequencies above 1600 Hz required samples of a diameter of 29 mm, where the size of the CS particles becomes prominent compared to the diameter of the samples. Thus, the results obtained for absorption at high frequencies (Fig. 5) should be analyzed with caution. A more

bioresources.com

appropriate method to measure the high-frequency sound absorption properties of these materials could be the method presented by Cucharero *et al.* (2020), which requires relatively small samples (50×50 cm^2). This method will be considered in future related work.

The sound absorption coefficients presented in Figs. 4 and 5 can guide material producers to define the needed thickness of a porous absorber layer made of fibers and CSs-like particles to produce materials optimized to attenuate sound in the desired frequency range. For example, the acoustical design of rooms in which good speech intelligibility is needed requires sound-absorbing materials with high absorption properties at 500 Hz and above because speech contains important sound energy at frequencies above 500 Hz. Speech also contains sound energy at frequencies below 500 Hz, but these frequencies play a less relevant role in speech intelligibility. All the materials prepared in this study, except those made of only CSs, could be used to improve the acoustics of rooms where speech intelligibility is needed, such as classrooms or meeting rooms.

This study demonstrates how easily a sustainable option for traditional building materials could be developed with existing technologies. Fully bio-based sound absorber samples exhibited sufficient mechanical and acoustical properties for indoor use to function as an efficient acoustic product. Long-term testing and fire properties of the material were not in the scope of this study; however, these are necessary for building materials. Although the CSs content hindered the mechanical and acoustical properties of the absorbers, especially with high CSs contents, the CSs could be used to decrease the overall carbon footprint of the absorbers. Although the pulp is a carbon-negative raw material (Foroughi *et al.* 2021), the CSs are even more environmentally beneficial as they are a by-product of other processes and would otherwise be incinerated.

CONCLUSIONS

1. In this study, fully bio-based sound absorbers were produced, and they were shown to exhibit sufficient mechanical and acoustical properties to function as an acoustic product for indoor use. Such products in buildings decrease the carbon footprint, especially those materials with higher cutter shavings (CSs) contents.

2. The mechanical properties of the samples were determined mainly by the properties of the pulp fiber network. Increasing the cellulose powder (CP) content improved the mechanical properties of the materials slightly, but it did not affect the acoustical properties.

3. It was demonstrated that the sound absorption properties of these fully bio-based materials could be tuned by carefully selecting the CSs and fiber contents and adjusting the thickness of the materials. A greater CSs content could be considered to decrease the carbon footprint of the material; however, it also decreases the sound absorption properties of the material at lower frequencies. In contrast, increasing fiber content resulted in materials with greater sound absorption at lower frequencies. This greater absorption could be attributed to increased tortuosity, which led to acoustically thicker materials.

bioresources.com

ACKNOWLEDGMENTS

REFERENCES CITED

Alava, M., and Niskanen, K. (2006). "The physics of paper," *Rep. Prog. Phys.* 69(3), 669-723. DOI: 10.1088/0034-4885/69/3/R03

Ashby, M. F. (1983). "The mechanical properties of cellular solids," *Metall. Mater. Trans. A* 14A, 1755-1769. DOI: 10.1007/BF02645546

Attenborough, K. (1971). "The influence of microstructure on propagation in porous fibrous absorbents," *J. Sound Vib.* 16(3), 419-442. DOI: 10.1016/0022-460X(71)90597-9

Botterman, B., de la Grée, G. C. H., Hornikx, M. C. J., Yu, Q. L., and Brouwers, H. J. H. (2018). "Modelling and optimization of the sound absorption of wood-wool cement boards," *Appl. Acoust.* 129, 144-154. DOI: 10.1016/j.apacoust.2017.07.017

Celzard, A., Zhao, W., Pizzi, A., and Fierro, V. (2010). "Mechanical properties of tannin-based rigid foams undergoing compression," *Mater. Sci. Eng. A* 527(16-17), 4438-4446. DOI: 10.1016/j.msea.2010.03.091

Cucharero, J., Ceccherini, S., Maloney, T., Lokki, T., and Hänninen, T. (2021). "Sound absorption properties of wood-based pulp fibre foams," *Cellulose* 28, 4267-4279. DOI: 10.1007/s10570-021-03774-1

Cucharero, J., Hänninen, T., and Lokki, T. (2020). "Angle-dependent absorption of sound on porous materials," *Acoustics* 2(4), 753-765. DOI: 10.3390/acoustics2040041

Dong, K., Wang, X., and Yang, J. (2021). "Predicting model of sound absorbing properties of cellulose-based porous materials prepared by foam forming," *J. Nat. Fibers*, article ID: 1990178. DOI: 10.1080/15440478.2021.1990178

Fahy, F. J. (2000). "Sound absorption and sound absorbers," in: *Foundations of Engineering Acoustics*, Elsevier Academic Press, London, UK, pp. 140-180.

Ferreira, E. S., and Rezende, C. A. (2018). "Simple preparation of cellulosic lightweight materials from eucalyptus pulp," *ACS Sustain. Chem. Eng.* 6(11), 14365-14373. DOI: 10.1021/acssuschemeng.8b03071

Foroughi, F., Rezvani Ghomi, E., Morshedi Dehaghi, F., Borayek, R., and Ramakrishna, S. (2021). "A review on the life cycle assessment of cellulose: From properties to the potential of making it a low carbon material," *Materials* 14(4), article 714. DOI: 10.3390/ma14040714

Garcia, C. A., and Hora, G. (2017). "State-of-the-art of waste wood supply chain in Germany and selected European countries," *Waste Manage.* 70, 189-197. DOI: 10.1016/j.wasman.2017.09.025

Hassan, M. K., Villa, A., Kuittinen, S., Jänis, J., and Pappinen, A. (2019). "An assessment of side-stream generation from Finnish forest industry," *J. Mater. Cycles Waste Manag.* 21, 265-280. DOI: 10.1007/s10163-018-0787-5

Hjelt, T., Ketoja, J. A., Kiiskinen, H., Koponen, A. I., and Pääkkönen, E. (2022). "Foam forming of fiber products: A review," *J. Dispers. Sci. Technol.* 43(10), 1462-1497. DOI: 10.1080/01932691.2020.1869035

Hill, C. A. S. (2019). "The environmental consequences concerning the use of timber in the built environment," *Front. Built Environ.* 5, article 129. DOI: 10.3389/fbuil.2019.00129

Ibn-Mohammed, T., Greenough, R., Taylor, S., Ozawa-Meida, L., and Acquaye, A. (2013). "Operational *vs.* embodied emissions in buildings—A review of current trends," *Energ. Buildings* 66, 232-245. DOI: 10.1016/j.enbuild.2013.07.026

Jahangiri, P., Logawa, B., Korehei, R., Hodgson, M., Martinez, D. M., and Olson, J. A. (2016). "On acoustical properties of novel foam-formed cellulose-based material," *Nord. Pulp Pap. Res. J.* 31(1), 14-19. DOI: 10.3183/npprj-2016-31-01-p014-019

Ketoja, J. A., Paunonen, S., Jetsu, P., and Pääkkönen, E. (2019). "Compression strength mechanisms of low-density fibrous materials," *Materials* 12(3), article 384. DOI: 10.3390/ma12030384

Lappalainen, T., and Lehmonen, J. (2012). "Determinations of bubble size distribution of foam-fibre mixture using circular Hough transform," *Nord. Pulp Pap. Res. J.* 27(5), 930-939. DOI: 10.3183/NPPRJ-2012-27-05-p930-939

Notley, S. M., and Norgren, M. (2006). "Measurement of interaction forces between lignin and cellulose as a function of aqueous electrolyte solution conditions," *Langmuir* 22(26), 11199-11204. DOI: 10.1021/la0618566

Paunonen, S., Timofeev, O., Torvinen, K., Turpeinen, T., and Ketoja, J. A. (2018). "Improving compression recovery of foam-formed fiber materials," *BioResources* 13(2), 4058-4074. DOI: 10.15376/biores.13.2.4058-4074

Pöhler, T., Jetsu, P., and Isomoisio, H. (2016). "Benchmarking new wood fibre-based sound absorbing material made with a foam-forming technique," *Build. Acoust.* 23(3-4), 131-143. DOI: 10.1177/1351010X16661564

Pöhler, T., Ketoja, J. A., Lappalainen, T., Luukkainen, V. M., Nurminen, I., Lahtinen, P., and Torvinen, K. (2020). "On the strength improvement of lightweight fibre networks by polymers, fibrils and fines," *Cellulose* 27, 6961-6976. DOI: 10.1007/s10570-020-03263-x

SFS-EN 826 (2013). "Thermal insulating products for building applications - Determination of compression behaviour," Finnish Standards Association SFS ry, Helsinki, Finland.

SFS-EN ISO 10534-2 (2001). "Acoustics - Determination of sound absorption coefficient and impedance in impedance tubes - Part 2: Transfer-function method (ISO 10534-2:1998)," Finnish Standards Association SFS ry, Helsinki, Finland.

Swift, M. J., Briš, P., and Horoshenkov, K. V. (1999). "Acoustic absorption in re-cycled rubber granulate," *Appl. Acoust.* 57(3), 203-212. DOI: 10.1016/S0003-682X(98)00061-9

Yamaguchi, M., Nakagawa, H., and Mizuno, T. (1999). "Sound absorption mechanism of porous asphalt pavement," *J. Acoust. Soc. Jpn. (E)* 20(1), 29-43. DOI: 10.1250/ast.20.29
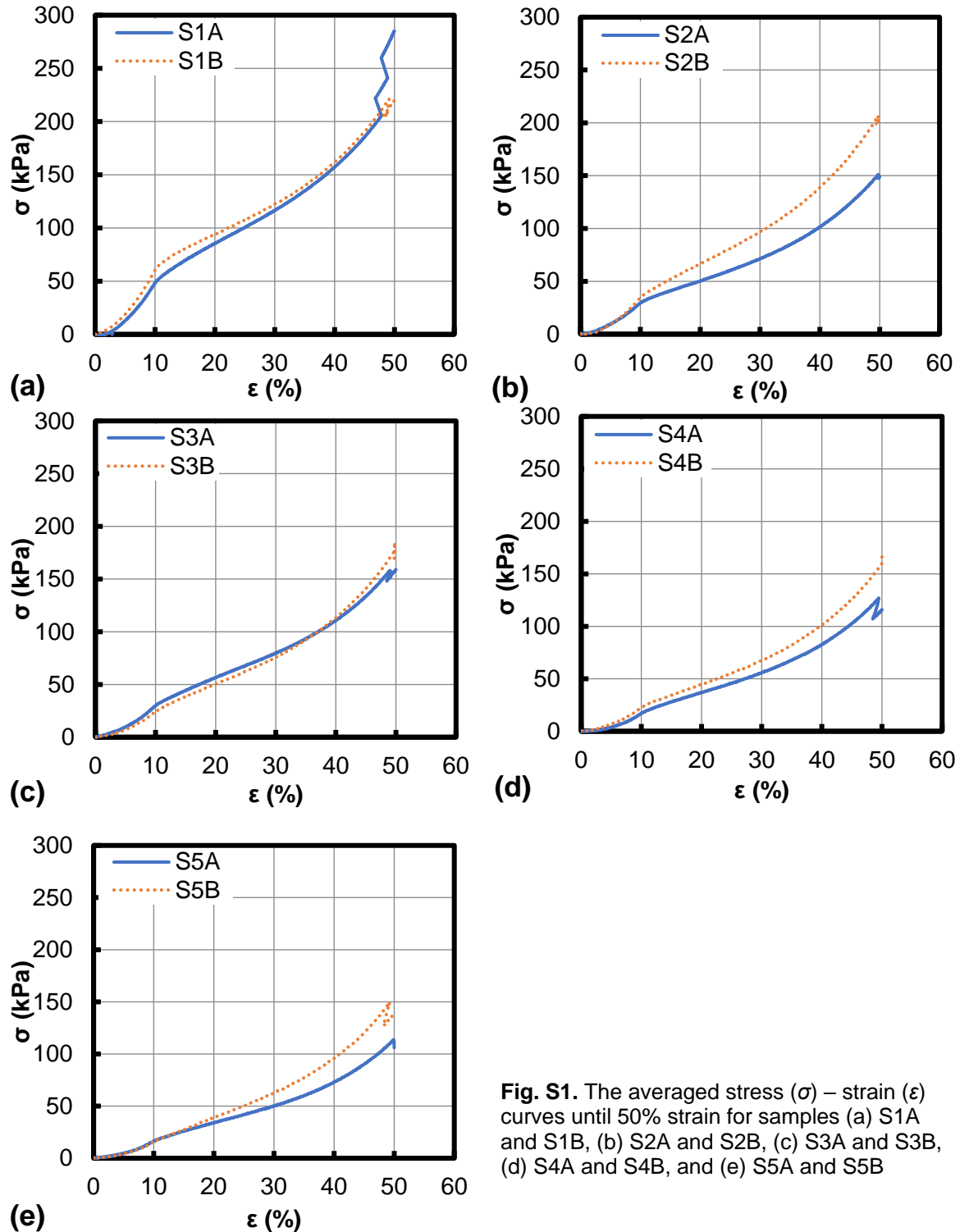
APPENDIX

Supplementary Material

Fig. S1. The averaged stress (σ) – strain (ε) curves until 50% strain for samples (a) S1A and S1B, (b) S2A and S2B, (c) S3A and S3B, (d) S4A and S4B, and (e) S5A and S5B